Characterization of edge poloidal impurity asymmetries at ASDEX Upgrade

D.J. Cruz-Zabala[1,2], E. Viezzer[1,2], U. Plank[3], R. M. McDermott[3], M. Cavedon[3], R. Dux[3], P. Cano-Megias[4,2], T. Pütterich[3], A. Jansen van Vuuren[1,2], J. Garcia-Lopez[1,2], M. Garcia-Munoz[1,2], and ASDEX Upgrade team

[1] *Dept. of Atomic, Molecular and Nuclear Physics, University of Seville, Seville, Spain*

[2] *CNA (U. Sevilla, CSIC, J. de Andalucia), Seville, Spain*

[3] *Max-Planck-Institut für Plasmaphysik, Garching, Germany*

[4] *Dept. of Energy Engineering, University of Seville, Seville, Spain*

Introduction. Future fusion reactors will require impurities as actuators to reduce the thermal loads to the first wall (via radiation). To understand how the impurities distribute in the plasma, detailed impurity measurements are needed. Impurity properties are commonly obtained with the Charge eXchange Recombination Spectroscopy (CXRS) technique. This technique takes advantage of the light emitted after the charge exchange reaction between an injected neutral and an impurity of the plasma. Normally, these measurements are performed using a neutral beam injection (NBI) system as the source of neutrals and provide measurements at the Low Field Side (LFS). Gas puff based systems provide the flexibility to make CXRS measurements where an NBI system is not suitable. At ASDEX Upgrade, two gas puff based CXRS systems are installed: one at the LFS and one at the High Field Side (HFS) [1] allowing the study of the impurity properties at two different positions in the plasma. In previous studies [2,3,4,5], it was shown that in order to explain the LFS/HFS asymmetries observed in the rotation profiles at the plasma edge, the impurity density can not be a flux function. Figure [1] shows an example of the experimental and the expected, edge HFS parallel rotation profiles, the latter calculated assuming that the impurity density is constant along the flux surfaces [3]. In this work, edge impurity density asymmetries will be studied by means of the upgraded gas puff based CXRS diagnostics and a new gas puff module implemented in the FIDASIM code [6].

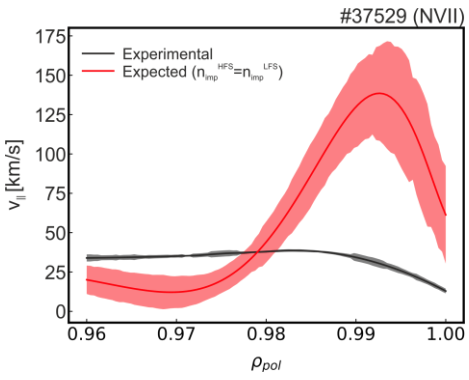

Figure 1. Experimental and expected HFS edge parallel velocity.

Impurity measurements at the HFS and LFS. Figure 2 shows the experimental impurity profiles obtained during an H-mode discharge at ASDEX Upgrade (shot #37529). This

discharge features a magnetic field of -2.5 T and a plasma current of 1.0 MA. 4.85 MW of NBI and 1.35 MW of ECRH were applied. The electron density at the pedestal top was $6.5 \cdot 10^{19}$ m^{-3}. Several CXRS diagnostics were used: LFS beam based (toroidal and poloidal views), LFS gas puff based (poloidal view) and HFS gas puff based (toroidal and poloidal views). The different diagnostics were aligned such that the maximum temperature gradients match [7]. This results in a shift of -3 mm to the toroidal LFS beam based system and a shift of 2 mm to the HFS gas puff based systems (toroidal and poloidal). The temperature shows a similar shape between HFS and LFS. The toroidal rotation shows a different behaviour between HFS and LFS: it has a maximum at the HFS close to the temperature pedestal top and it has a minimum at the LFS at a slightly different position. The poloidal rotation shows a negative minimum at both the LFS and HFS, although the HFS minimum is smaller in magnitude. In this work, positive poloidal velocities go in the ion diamagnetic drift direction.

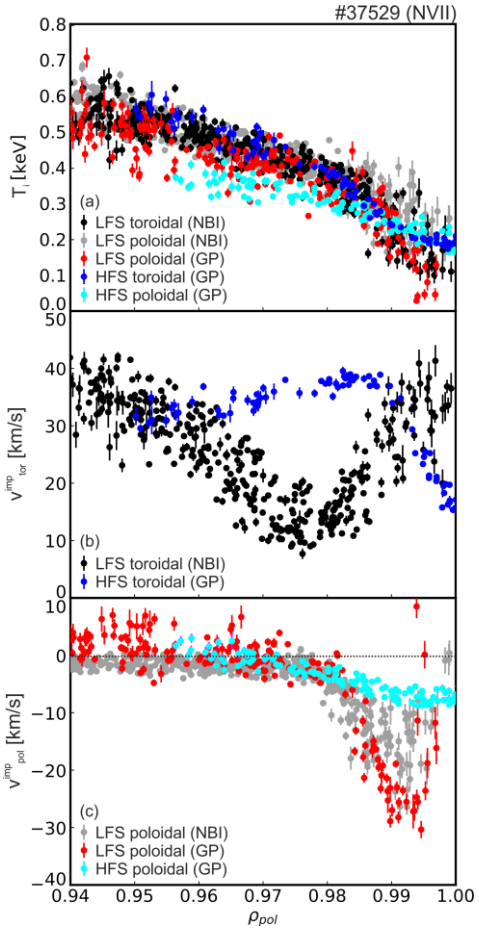

Figure 2. Temperature, toroidal rotation and poloidal rotation profiles.

Gas puff modelling in FIDASIM. In order to enable the impurity density calculation from gas puff based CXRS systems, a new gas puff module has been included in the FIDASIM code [6]. This model launches Monte Carlo markers that follow the initial distribution observed during laboratory tests [1]. Figure 3 shows the 3D and 2D initial unit vector distributions. The valve injection goes in the z direction. In the experiments, D_2 molecules are injected. The model assumes that each molecule dissociates rapidly into two atoms, one going towards

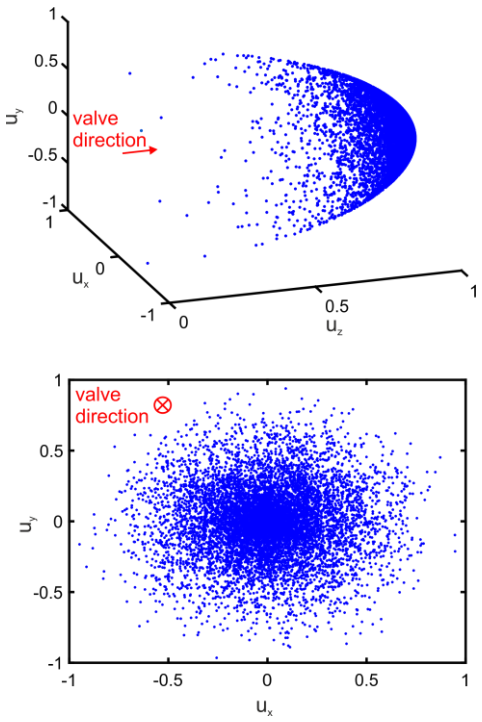

Figure 3. 3D and 2D initial unit vector distribution of the markers. Injection direction goes in the z direction.

the plasma and one going towards the wall [8]. Due to the low energy of the injected neutrals, they are ionized before reaching the confined region. However, successive generation of neutrals can be produced after the charge exchange of an injected neutral and a main ion. This produces a new generation of neutrals called halo neutrals. This process has to be treated in different steps as additional generations of halo neutrals can be produced after the charge exchange of a halo neutral from a previous generation and a main ion. These successive generations of halo neutrals form the population that penetrates into the confined region of the plasma. The distribution of the injected neutrals and halo neutrals produced by the HFS gas puff system as calculated with the new gas puff module is shown in figure 4.

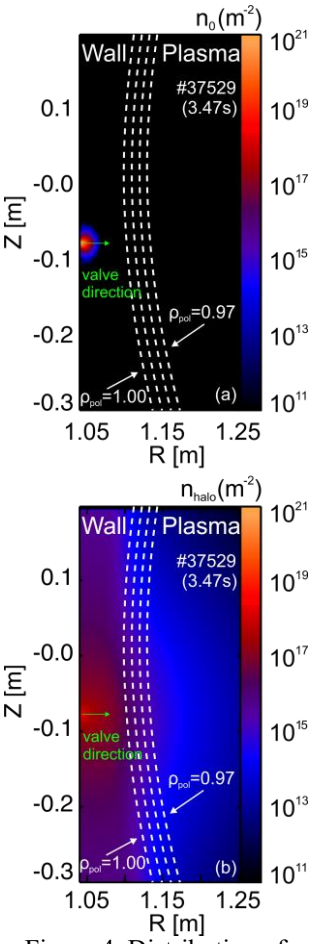

Figure 4. Distribution of injected neutrals and halo neutrals

Impurity density calculation. As the halo neutrals are the population penetrating into the plasma, they will play a dominant role for the charge exchange reactions with impurities. The new gas puff module has been included in the CHICA code [9]. CHICA uses the neutrals from FIDASIM and the radiance $L_{CX,z,\lambda}$ of the CXRS diagnostic to obtain the impurity density:

$$n_z = \frac{4\pi}{h\nu} \frac{L_{CX,z,\lambda}}{\sum_n \int_{LOS} n_{D,n}(s) \langle \sigma_{n,Z,\lambda} v_j \rangle_{eff}(s) ds}$$

The impurity density calculated using the LFS gas puff based CXRS system has been benchmarked against well-established impurity density calculations from beam based CXRS systems. Figure 5 shows such a comparison for the BV (494.5 nm) and the NVII (567.0 nm) lines. Good agreement has been found in both cases, validating the new module.

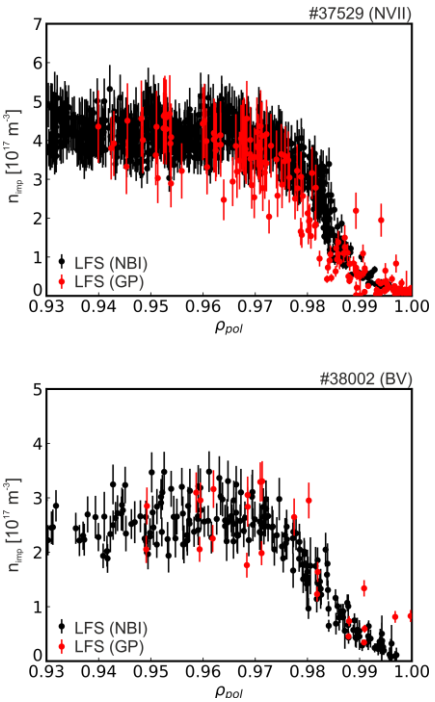

Figure 5. Comparison of the impurity density profile between LFS beam based CXRS and LFS gas puff based CXRS

Impurity density asymmetries. The impurity density is evaluated from the HFS and LFS gas-puff CXRS measurements and the new gas puff module implemented in FIDASIM. An estimation of the asymmetry factor

$n_{imp}^{HFS}/n_{imp}^{LFS}$ can be obtained from the flow measurements following the procedure shown in [2,3]:

$$\frac{n_{imp}^{HFS}}{n_{imp}^{LFS}}_{flows} \approx \frac{\left[v_{||,\alpha,LFS}^{exp} - \frac{v_{\perp,\alpha,LFS}^{exp}}{\sin\delta_{LFS}}\right]\frac{B_{HFS}}{B_{LFS}}}{v_{||,\alpha,HFS}^{exp} - \frac{v_{\perp,\alpha,LFS}^{exp}}{\sin\delta_{LFS}}\frac{R_{HFS}}{R_{LFS}}}$$

Figure 6 shows the impurity density at the HFS and at the LFS and the asymmetry factor obtained from density measurements (using the new gas puff module) and estimated from the flow measurements of nitrogen (shot #37529). Excellent agreement has been found between the asymmetry factor from density and flow measurements showing in both cases that the impurities tend to accumulate at the HFS, consistent with previous studies [2,3,4,5]. This new gas puff module allows us to calculate the impurity density asymmetries in scenarios without NBI.

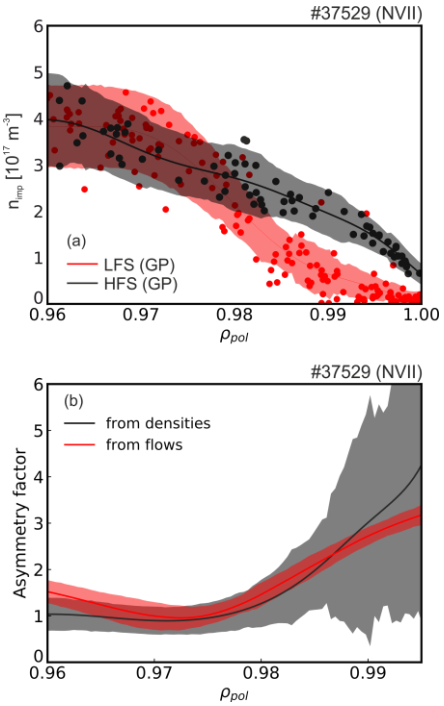

Figure 6. Comparison of the impurity density between HFS and LFS and asymmetry factor obtained from density and from flow measurements.

Conclusions. A new gas puff module has been included in the FIDASIM code in order to study edge poloidal impurity density asymmetries. The impurity density calculation shows that the impurities tend to accumulate at the HFS. This result agrees with the impurity density asymmetries needed to explain the flow structure.

Acknowledgements. This work received funding from the VI Plan Propio de Investigación de la Universidad de Sevilla (PPITUS 2017). This work has been carried out within the framework of the EUROfusion Consortium and has received funding from the Euratom research and training programme 2014-2018 and 2019-2020 under grant agreement No 633053. The views and opinions expressed herein do not necessarily reflect those of the European Commission.

References

[1] D.J. Cruz-Zabala et al. Journal of Instrumentation, 14:C11006, 2019

[2] K.D Marr et al. Plasma Physics and Controlled Fusion, 52:055010, 2010

[3] T. Pütterich et al. Nuclear Fusion, 52:083013, 2012

[4] E. Viezzer et al. Nuclear Fusion, 55:123002, 2015

[5] R.M. Churchill et al. Nuclear Fusion, 53:122002, 2013

[6] B. Geiger et al, Plasma Phys. Control. Fusion 62: 105008 (2020).

[7] P.A. Schneider et al. Nuclear Fusion, 53:073039, 2013.

[8] R.M. Churchill et al. Review of Scientific Instruments, 84, 093505, 2013

[9] R.M. McDermott et al. Plasma Phys. Control. Fusion, 60:095007, 2018